

CERN/PS/BR/77-8
25 February 1977

[REDACTED]

CERN LIBRARIES, GENEVA



CM-P00059561

THEORY AND PERFORMANCE OF THE LONGITUDINAL ACTIVE DAMPING SYSTEM
FOR THE CERN PS BOOSTER

F. Pedersen and F. Sacherer
CERN, Geneva, Switzerland

Presented at the
7th National Particle Accelerator Conference,
Chicago, 16-18 March 1977

THEORY AND PERFORMANCE OF THE LONGITUDINAL ACTIVE DAMPING SYSTEM
FOR THE CERN PS BOOSTER

F. Pedersen and F. Sacherer
CERN, Geneva, Switzerland

Introduction and Summary

Longitudinal instabilities have long been troublesome in the Booster¹). They are described by the coupled-bunch mode number $n = 0$ to 4 for five bunches, and by the within-bunch mode number $m = 1$ for dipole, $m = 2$ for quadrupole, $m = 3$ for sextupole, and so on (Fig. 1). The normal beam control system damps the rigid-bunch oscillation ($n=1$) when all five bunches move together ($n=0$)²). The new feedback system³ damps the other coupled-bunch modes $n = 1$ to 4 for the three lowest orders, $m = 1$ to 3. With the damping system off, one can display the evolution of any mode along the cycle, which helps in locating coupling impedances that cause instability. One can also excite the various modes and measure the amplitude-phase response (RF knockout applied to a bunched beam). This gives the frequency spread within the bunch, the coherent frequent shifts, plus the usual stability diagram in the U-V plane.

Modes of Oscillation

It is evident from Figs. 1a and 1b that the line density $\lambda(t)$ of a bunch can be decomposed into two parts, the stationary distribution $\lambda_0(t)$ plus an additional charge density $\lambda_m(t)$ oscillating at m times the synchrotron frequency⁴). The oscillating part $\lambda_m(t)$ is an approximately sinusoidal standing-wave pattern with m fixed nodes along the bunch:

$$\lambda_0(t) + \lambda_m(t) \quad m = 2$$

In addition, the different bunches may be coupled together. For M bunches, there are M coupled-bunch modes, designated by the index n . For identical, equally spaced bunches, $2\pi n/M$ is the phase difference between adjacent bunches. The modes can also be identified by the lines that occur in the bunch spectrum, namely

$$f_p = |(n + pM)f_0 + mf_s|, \quad -M < p < M \quad (1)$$

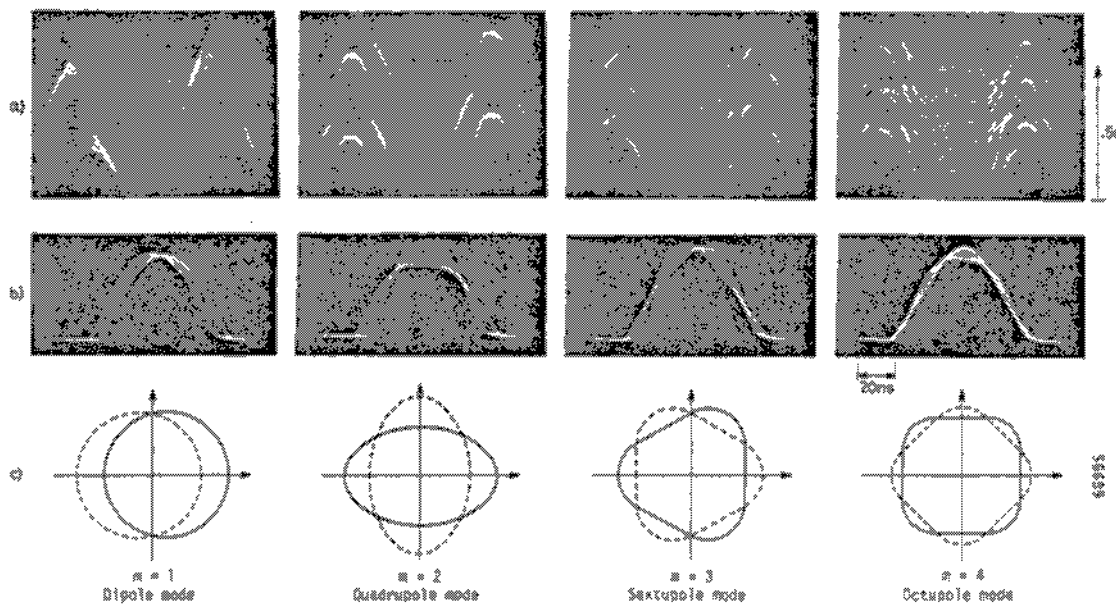


Fig. 1 Within-bunch modes $m = 1$ to 4, coupled-bunch mode pattern $n = 4$. a) Mountain-range display of one synchrotron period; b) Superimposed; c) Phase space.

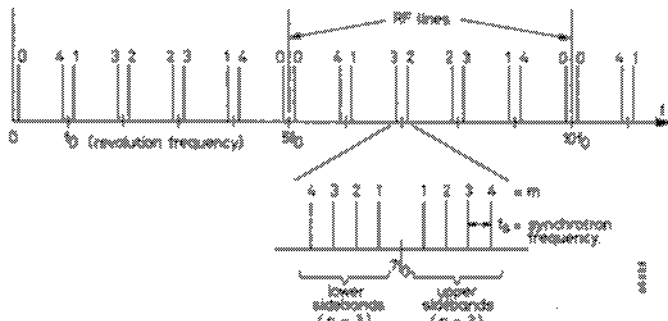


Fig. 2

where f_0 is the revolution frequency and f_s is the synchrotron frequency. These are shown in Fig. 2 for $M=5$ bunches. The lower sidebands are given by negative values of p . Figure 3 shows a measured spectrum, where the bandwidth (300 kHz) is too large to resolve the synchrotron frequency sidebands at mf_s ($f_s = 2$ kHz). The large

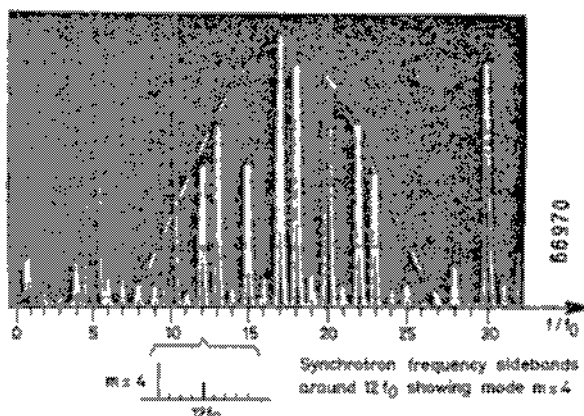


Fig. 3 Observed spectrum for mode $n=3$, $m=4$. Sweep speed 2 msec/div, bandwidth 300 kHz, range 0-50 MHz, linear scale, bunch length $\tau_L = 66$ nsec.

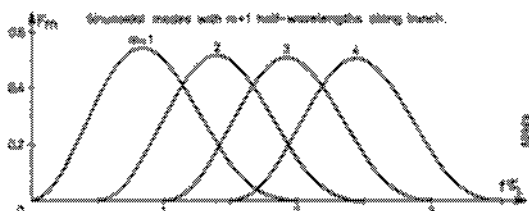


Fig. 4

lines at multiples of the radio frequency $5f_0$ are due to the stationary bunch distribution $\lambda_0(t)$. Smaller unequal-bunch lines also occur at harmonics of the revolution frequency f_0 if the five bunches are not identical.

The envelope of the spectrum is determined by the Fourier transform $\lambda(\omega)$ of $\lambda_0(t)$, namely $\lambda_0(\omega)$ for the RF lines and $\lambda_m(\omega)$ for the sideband spectra. The normalized power spectrum

$$F_m = \frac{1}{M\Omega_0} \sum_p \frac{|\lambda_m(p)|^2}{\lambda_0(p)} \quad (2)$$

is shown in Fig. 4 for the case where $\lambda_0(t)$ is assumed to be a sine wave with $m+1$ half-wavelengths along the bunch. The bunching factor $B_B = \text{bunch length } T_B/\text{revolution period } T$ is included so that the magnitude of F_m is independent of bunch length. The actual spectrum taken from photographs such as Fig. 3 is shown in Fig. 5. As one can see, the measured spectrum is shifted down in frequency, and the reason is evident from Fig. 1b, namely mode m has fewer than $m+1$ half-wavelengths. For example, the octupole mode has 4 nodes and only ~ 3.5 half-wavelengths. With this correction, a good fit is obtained for the spectrum (dashed curve in Fig. 3).

Growth-rate Formula

The growth rate is given by $-\text{Im } \Delta\omega_{m,n}$ where

$$\Delta\omega_{m,n} = j \frac{m\pi}{m+1} \frac{I}{38\pi hV \cos \phi_s} \sum_p F_m \frac{Z}{p} \quad (3)$$

and the form factor F_m and coupling impedance Z are evaluated at the frequencies f_p given by Eq. (1). Here I is the total current in M bunches; ω_0 is the synchrotron frequency in rad/sec; h is the RF harmonic number; $V \sin \phi_s$ is the voltage gain per turn, with the convention that $\cos \phi_s$ is positive below transition and negative above; the usual convention is used for Z , namely inductive impedance jZ has positive reactance. The signs in Eq. (3) are such that lower sidebands are unstable below transition, upper sidebands are stable, and the opposite is true above transition. For a narrow impedance Z , only one frequency f_p contributes to the sum in Eq. (3).

Active Feedback

The signal from a longitudinal pick-up is fed back to the RF accelerating cavity through two tracking filters centred on the 6th and 7th harmonics of the revolution frequency (Fig. 6). The effective impedances (cavity voltage/beam current at the cavity) of the two transfer functions have positive resistive part for upper sidebands and negative resistive part for lower sidebands (Fig. 6) to damp both upper and lower sidebands, $n=1,4$ and $2,3$, and a sufficient width to include modes $m=1$ to 3 . The choice of $6f_0$ and $7f_0$ ensures that the form factors F_m are relatively large for modes $m=1$ to 3 (Fig. 5), that the time delays are manageable, and that the impedance of the RF cavity tuned to $5f_0$ is still sufficient. Typical measured damping rates are (at 600 Mev):

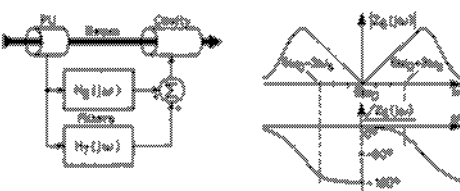


Fig. 6 Active feedback and equivalent impedance

tion frequency (Fig. 6). The effective impedances (cavity voltage/beam current at the cavity) of the two transfer functions have positive resistive part for upper sidebands and negative resistive part for lower sidebands (Fig. 6) to damp both upper and lower sidebands, $n=1,4$ and $2,3$, and a sufficient width to include modes $m=1$ to 3 . The choice of $6f_0$ and $7f_0$ ensures that the form factors F_m are relatively large for modes $m=1$ to 3 (Fig. 5), that the time delays are manageable, and that the impedance of the RF cavity tuned to $5f_0$ is still sufficient. Typical measured damping rates are (at 600 Mev):

	$m = 1$ (sec $^{-1}$)	$m = 2$ (sec $^{-1}$)	$m = 3$ (sec $^{-1}$)
$n = 1,4$	370	400	60
$n = 2,3$	140	175	50



Fig. 7 Tracking mode analyser amplitude response

Mode Analyser

Four additional narrow-band tracking filters⁵ allow observation of the individual modes $n=1$ to 4 and $m=1$ to 4 (Fig. 7). An associated tracking drive system is used to drive up any desired mode (m and n), so that its growth or damping rate can be measured under clean conditions (Fig. 8). Some results of these measurements are shown in Fig. 9 for dipole and quadrupole modes during the last 250 msec of the cycle. The mode frequencies f_p are also shown. The predicted damping/antidamping symmetry for upper and lower sidebands ($n=1,4$ and $2,3$) is clearly visible, as well as the lowering of the growth-damping rates for quadrupole modes due to Landau damping.

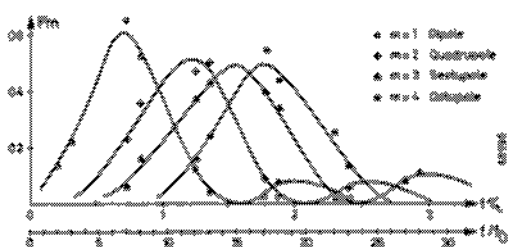


Fig. 5 Measured form factors F_m

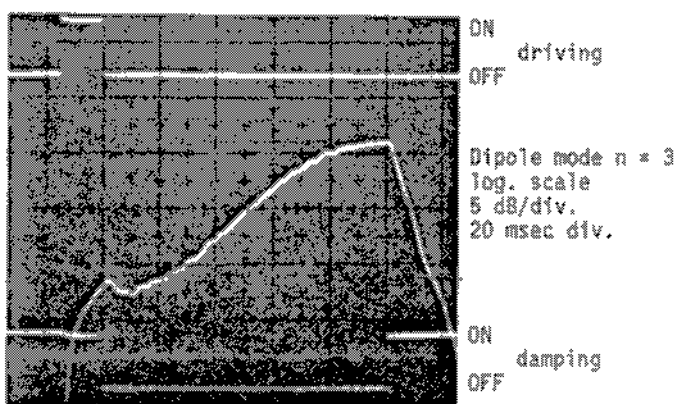


Fig. 8 Driving, free growth, and damping

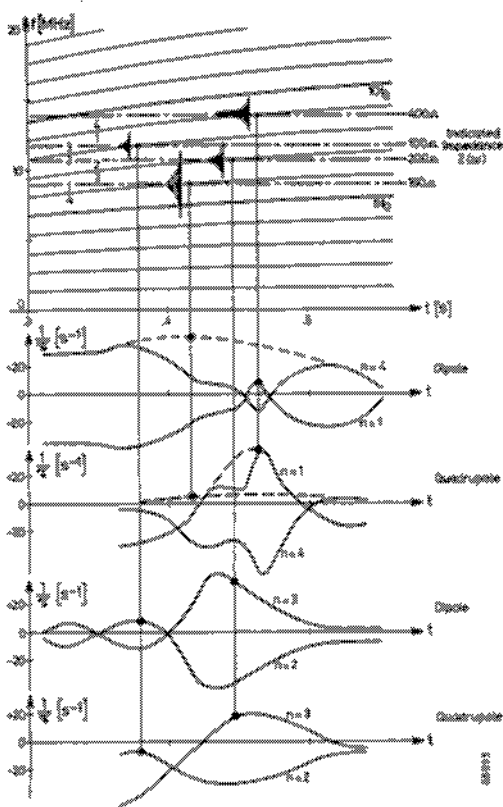


Fig. 9 Growth and damping rates for dipole and quadrupole modes (Ring 4 with 3.2×10^{12} protons)

The coupling impedances that cause the instabilities can be found from the growth/damping rates and the form factors (Fig. 5). There is evidently a broad impedance around 9 MHz that drives the $n = 4$ dipole mode, and more weakly the $n = 4$ quadrupole mode (because its form factor is smaller at $6f_0$). Superimposed is the effect of a narrower resonance around 14 MHz that damps $n = 4$ and drives $n = 1$, with about equal strength for dipole and quadrupole modes, since their form factors are about equal at 9%.

RF Excitation

The drive system, mode analyser, and a network analyser are used to measure the amplitude-phase response $A(j\omega)$ for the various modes (Fig. 10). The response deviates from that of a simple oscillator, especially when the drive frequency is within the band of incoherent synchrotron frequencies⁶. Care is required to ensure that the bunch distribution is not modified by the drive signal. The response was measured at fixed frequencies with drive levels just above the noise level and short drive times of 50 msec or less.

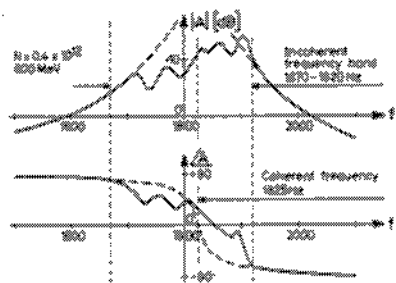


Fig. 10 RF knockout. Phase and amplitude response around $n = 3$ dipole sideband.

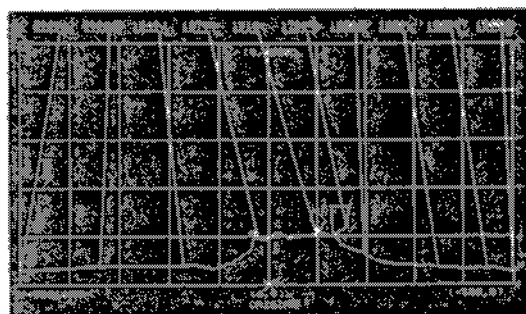


Fig. 11 Stability diagram for $n = 3$ dipole mode with damping on

Signal averaging (~ 10 averages) improved the signal-to-noise ratio.

The inverse function $1/A(j\omega)$ gives the usual stability diagram⁷ (Fig. 11). The origin is the coherent frequency, and the bump on the curves is the band of incoherent frequencies. In this case the damping was on, so the coherent frequency is shifted into the stable region (below the curve).

The measured incoherent frequency bands for dipole and quadrupole modes are shown in Fig. 12 for different intensities. They are shifted down by the strong space-charge forces. For intensities above 2×10^{12} protons per ring, dipole modes are no longer Landau damped, which fits well with the measured growth rates (Fig. 13). Higher intensities ($> 2.8 \times 10^{12}$ protons/ring) are required to shift the coherent quadrupole frequency out of the incoherent band, because it starts lower (larger amplitude particles are more important), and because space charge shifts it down. In summary, the very large space-charge shifts ($> 2000 \text{ sec}^{-1}$) move the coherent frequency out of the stable region, so that even relatively small resistive impedances of a few hundred ohms are harmful ($1/t < 50 \text{ sec}^{-1}$).

References

- 1) F. Gareyte et al., IEEE Trans. Nuclear Sci. NS-22, 1855 (1975).
- 2) G. Gelato and L. Magnani, Better dynamic closed loop control of the PSB RF accelerating system, these proceedings.
- 3) B. Kriegerbaum and P. Pedersen, Electronics for the longitudinal active damping system for the CERN PS Booster, these proceedings.
- 4) F.J. Sacherer, IEEE Trans. Nuclear Sci. NS-20, 825 (1973), and also these proceedings.
- 5) P. Asboe-Hansen, CERN/PS/OP 76-6 (1976).
- 6) G.H. Harward, CERN 65-20 (1965).
- 7) D. Möhl and A. Sessler, Proc. 8th Internat. Conf. on High-Energy Accelerators, CERN, Geneva, 1971 (CERN, Geneva, 1971), p. 334.

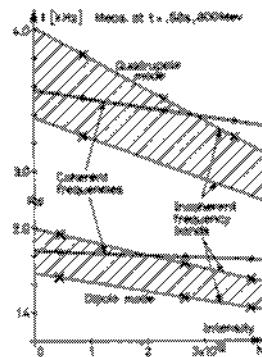


Fig. 12

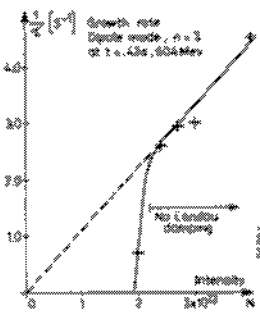


Fig. 13